The fiber positioner for 4MOST: exploration of an alternative R-θ design

Allar Saviauk*[a], Frank Dionies[a], Roelof de Jong[a], Roger Haynes[a], Ian Parry[b]

[a]Leibniz-Institut für Astrophysik Potsdam, An der Sternwarte 16, 14482 Potsdam, Germany;

[b]Institute of Astronomy, University of Cambridge, Madingley Road, Cambridge CB3 0HA, United Kingdom

ABSTRACT

We present a new type of R-θ fiber actuator named PotsPos for multi-object astronomical spectroscopy. It was initially intended to use as an alternative positioner design for the 4-meter Multi-Object Spectroscopic Telescope (4MOST). Although another tilting spine technology developed by the Australian Astronomical Observatory (AAO) is currently chosen for the 4MOST, PotsPos design has some technical advantages over other positioning technologies and might therefore be an attractive choice for future spectrographs. The design would be similar in positioning capabilities to the tilting spine design but would not suffer from telecentricity and defocus errors. The mechanical design, suitable motors, computational results from dynamic simulations and finite element analyses are presented.

Keywords: 4MOST, multi-object spectroscopy, fiber positioner, fiber actuator, nonlinear finite element analysis, ANSYS

1. INTRODUCTION

Multi-object spectroscopy is an essential tool for astronomy carrying out large astronomical surveys containing thousands or even millions of spectra. Many multi-object spectrographs rely on optical fibers that need to be positioned to locations where the objects of interest are focused on the focal surface of the telescope. We present a design of a new type of fiber actuator named PotsPos (Potsdam Fiber Positioner) that is developed especially for the needs of the 4-meter Multi-Object Spectroscopic Telescope (4MOST). 4MOST is to be installed on the 4-meter ESO telescope VISTA in Chile. The instrument will position ~2400 optical fibers in 2,5 degree diameter FoV with precision of <10µm. Due to the large number of fibers and densely populated field plate a parallel positioner concept is favored over sequential design. In the parallel positioning scheme the fibers can be allocated independently which greatly reduces fiber configuration times. Just like the Echidna FMOS tilting spine design developed by the Australian Astronomical Observatory, PotsPos actuator has a large fill factor, large patrol area and good fiber-target assignment flexibility but would not suffer from telecentricity and defocus errors. This significantly reduces the light losses introduced in by the focal ratio degradation (FRD) and defocus effects. However, even the proposed positioner concept to be used for the 4MOST is the tilting spine design, PotsPos might still be an attractive choice for future positioners.

2. MAIN PRINCIPLE AND EARLY DEVELOPMENTS

The main drivers for the new actuator design came from a need to have a densely populated field plate (Echidna-like grid-based configuration) but to minimize the fiber tilt angle and to increase the patrol area. It was also necessary to keep the actuator design as short as possible because of the limited available space at the VISTA cassegrain focus. A high fill factor could be also achieved with a Theta-Phi style of actuator where the fiber is positioned by means of two rotational motors with one offset from the other (actuators like Cobra and MuPos). However, in this case there is very little overlap between the actuator patrol areas and the fiber-target assignment flexibility and field coverage would be significantly reduced. A drawback of densely packed fixed grid actuator concepts is that it's not very well suited for highly clustered fields since only a certain number of fibers are available for each area on the field plate.

*asaviauk@aip.de; phone +49 331 7499 397; www.aip.de

The PotsPos actuator is based on the R-Theta design meaning that it has one linear and one rotational movement (see Fig. 1). The main difference compared to other positioner designs is that the PotsPos is using the last element of the telescope's Wide Field Corrector (WFC) as a reference surface. The great advantage of this is that of five contributing degrees of freedom (x, y, z, tip, tilt), z (focus) is passively controlled by the reference surface. Furthermore, by careful design of the elements the tip can be compensated to some extent to follow the shape of the reference surface. This leads to the fact that only x and y needs to be under active control since tilt is constrained mechanically. The mechanism is folded in one plane to minimize the size of collision avoidance zones and hence fiber-target assignment flexibility is improved.[1]

The early proposal of the PotsPos actuator design took advantage of pre-loaded flexures (Fig. 1). The design was relatively simple and could be manufactured using 3D-printing technologies. One plastic (ABS) prototype was manufactured but the structure was found to be too fragile due to hard 3D-printed hinges that didn't allow much deformation. Next a metallic version with slightly modified flexures was considered but Finite Element Analysis (FEA) showed too much stress in the flexures. If the flexures are designed weaker allowing more deformation, the system becomes more spring-like and hysteresis would increase rapidly preventing precise prediction of fiber locations. Another issue with the metallic design was that the piezo actuators were not strong enough to sufficiently move the elements.

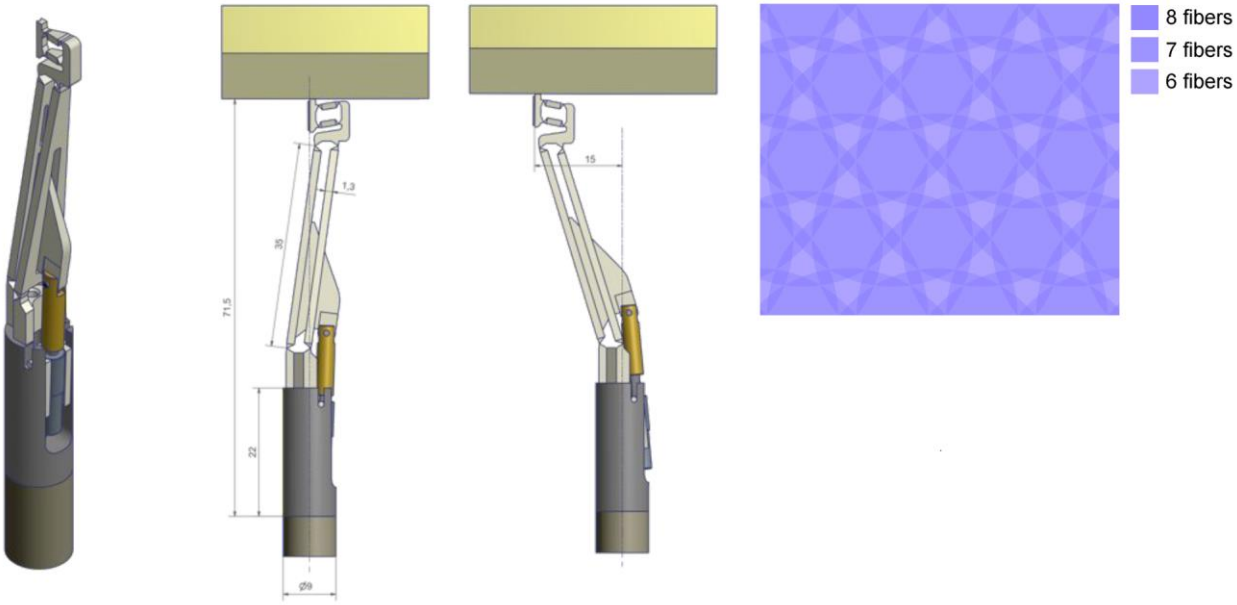

Figure 1. The early proposal of the PotsPos actuator design takes advantage of thin flexures. On the right is the patrol area of a PotsPos actuator indicating how many fibers can be placed on each point on a telescope's focal plane. In reality the pattern is more complex since collision avoidance zones are not subtracted from the pattern.

In principle each point on a telescope's focal plane can be reached by at least 6 actuators (edge of the field excluded). Most of the focal surface can be reached by 7 actuators and there are some smaller areas where 8 actuators can be placed. The Fig. 1 (right) illustrates the patrol area pattern when 10mm actuator pitch in a regular hexagonal grid with a 28mm patrol area diameter for each individual actuator is used. However, the illustrated pattern is simplified since it does not take to account collision avoidance zones that need to be subtracted from the pattern. The minimum distance between two adjacent fibers in the latest design is 0,6mm limited by the diameter of the fiber end cap shown in the Fig. 2. 0,6mm on the focal plane corresponds to 10arcsec in the sky.

3. MECHANICAL DESIGN OF POTSPOS

To overcome the challenges with the early PotsPos design, the actuator was re-engineered. In the Fig. 2 one can see the proposed new design for PotsPos. The main difference is that all of the flexures are removed and play-free joints with very low resistance are used instead (friction alone). Additional extension springs and leaf springs have been used to still have a pre-loaded mechanism. The actuator is mounted on a telescope's field plate from its basis. In the end of the basis

there is a rotational motor which transfers the θ-motion to the foot by using the drive. There is a linear piezo actuator mounted into the foot that transfers linear movement to the wedge. The wedge then transfers the linear movement to rotational movement using the leg group. The leg group is a sub-assembly having the lever, back plate and two rods fixed together as one assembly. Together with the third rod the rotational movement is transferred into zx-movement of an upper assembly. The pre-loaded leaf spring assures that the fiber end cap made of Teflon is always in contact with the reference surface. There is a small air gap between the field-lens and the fiber entrance to prevent wavelength fringing. The optical fiber is terminated in a stainless steel or fused silica ferrule which is guided by the leaf spring and the hole in the upper assembly. The overall length of the actuator is currently 150mm but is not fixed.[2]

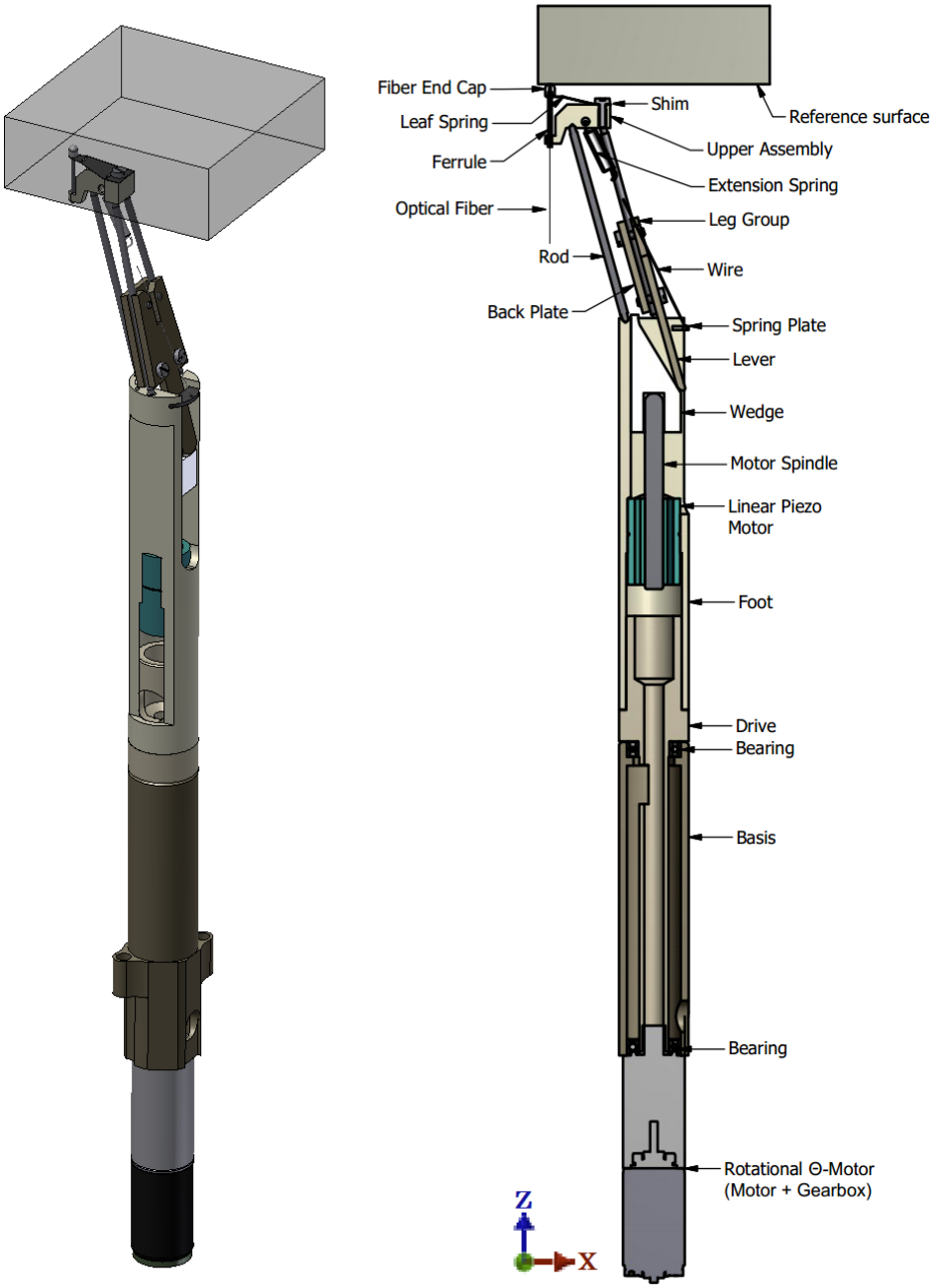

Figure 2. Mechanical design and elements of PotsPos actuator (hollow shafts in the motor and gearboxes not shown).

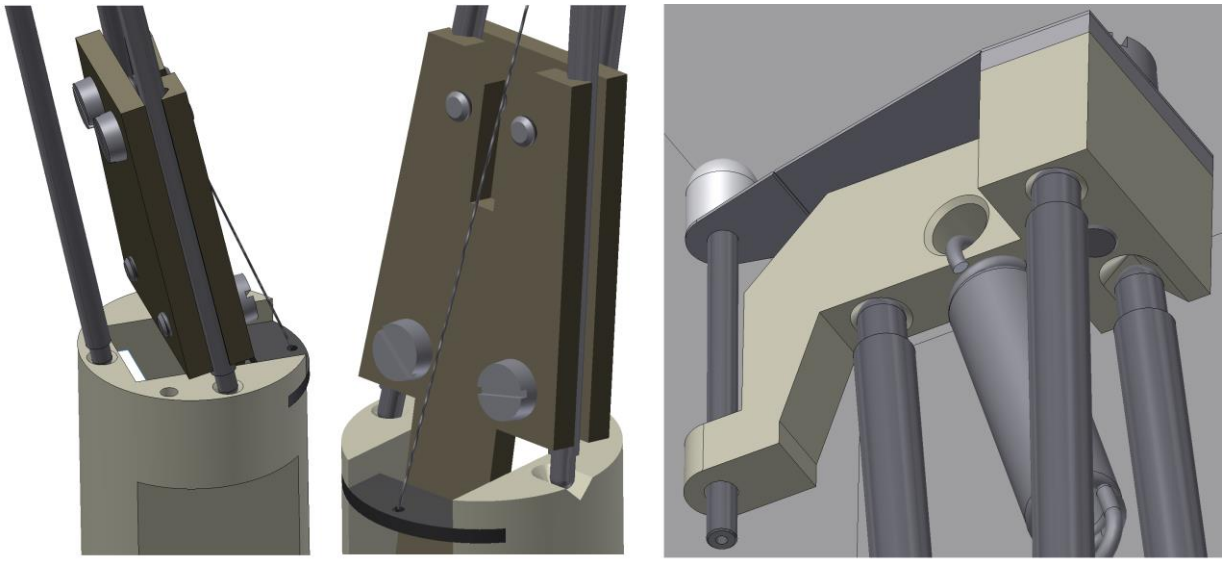

Figure 3. Detailed view to the joints. Spherical ball joints and combined joints in v-grooves are used to sufficiently constrain the mechanism.

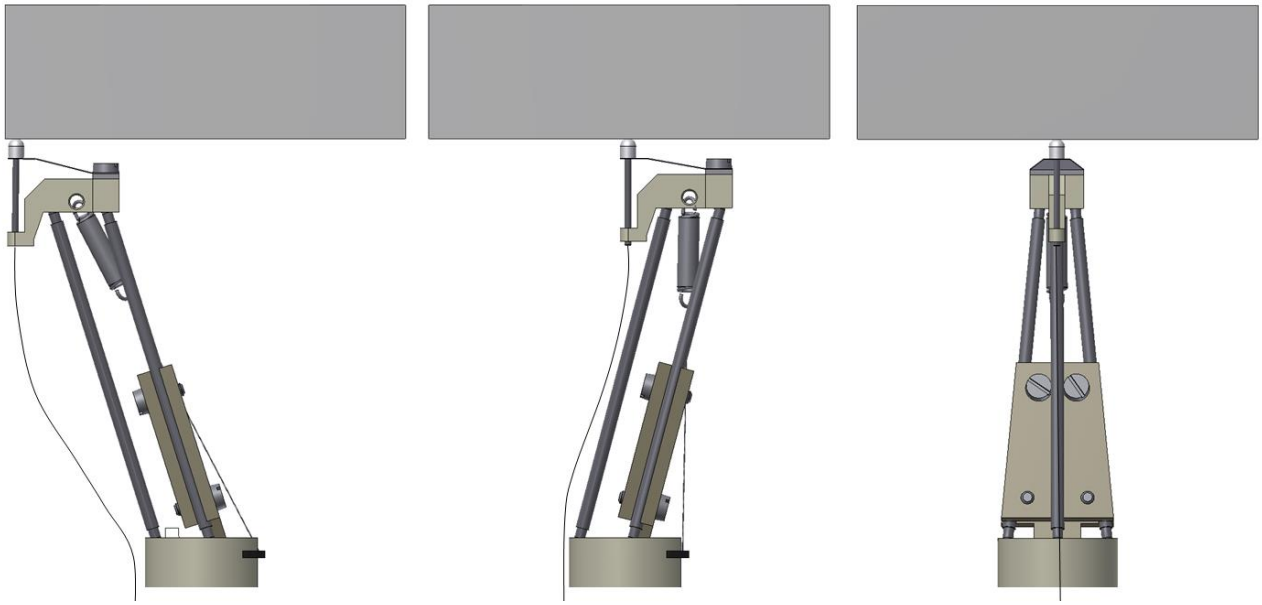

Figure 4. The first two figures illustrate the two extreme positions of PotsPos when the wedge is moved by its maximum 9mm distance (R-motion). This makes the total patrol area radius equivalent to 14,2mm. When in home position (middle), the tip of the fiber crosses the foot axis by 0,5mm. The right figure illustrates the θ-motion when rotated by 90°.

Two separated motors are needed to drive the actuator. The requirements for the linear motor are very demanding because of the small packaging size, high resolution, large travel length and relatively high force compared to the motor size. The only applicable motor for the R-motion was the SQUIGGLE® piezoelectric motor developed by New Scale Technologies Inc. The main specifications for this motor are listed in the Table 1.

Table 1. Manufacturers' specification for the SQUIGGLE Model SQL-3.4-10[3]

Specification	Value
Travel Range	7mm, 20mm
Housing Dimensions	Ø 6,83x11,02mm
Stator Dimensions	3,4x3,4x10mm
Stall Force	2N
Speed (at ½ stall force)	4mm/s
Resolution	0,5µm
Input Power when still	0W
Input Power when moving	1W
Lifetime	>70000 cycles (continuous operation, 1N stall force)
Operating temperature	-30°C - +70°C
Operating frequency	~115 KHz
Motor Weight	0,7g

For the rotational θ-motor the required positioning accuracy, small size and option to have a hollow shaft for fiber routing were the main drivers when selecting the motor. A combination of a stepper motor implemented with a small gearbox was selected. The motor is provided by Dr. Fritz Faulhaber GmbH & Co. KG[4]. To meet the positioning requirements and in order to keep the costs minimal the gearbox is a stack of one planetary gear and one harmonic drive. This leads to 0,47µm step size and ±0,84µm positioning accuracy at the maximum patrol radius 14,2mm (positioning errors in motor-gearbox assembly considered only). In principle a stack of two planetary gears would also meet the minimum step size requirement which is ±5µm but positioning errors exceeded the requirements by a factor of 2,5 due to backlash in the planetary gears. The backlash in planetary gears could be potentially eliminated by adding an additional preloading element into the system. The gears are provided by Micromotion GmbH. The company claimed that they are able to produce hollow shafts through the gears and the motor for fiber routing.

The idea was that the electrical cables and the optical fiber could run through the actuator to the other side of the focal plate. To achieve that there are some openings in the structure and in addition to the motor-gearbox assembly the drive is also hollow. However, the bend radii on optical fiber turned out to be unacceptably small and would introduce in significant light loss and FRD. Therefore the overall length of the actuator should be increased so that the bend radii become larger or preferably another solution to route the fiber should be found.

4. STATIC SIMULATIONS

In order to optimize the springs and the force on the linear motor faster, the Dynamic Simulation module of Inventor was used prior FEA. Slightly simplified 3D model of the actuator was simulated using virtual springs with different spring loadings. Because it was not possible to simulate the performance of the leaf spring in Inventor, a standard virtual compression spring was implemented instead. The leaf spring was still attached to the mechanism to include its mass. Different preload conditions and spring constants of the virtual springs were examined and their response on the force at the motor spindle was recorded.

Because the Dynamic Simulation module is somewhat limited, the output of the analysis corresponds to static conditions. The wedge was driven from its upper position down to its lower position by 9mm in 100 steps (Fig. 5). The Unknown Force- tool was used to calculate the required reaction force at the motor spindle at each step in order to achieve static equilibrium. Because each step was in static equilibrium it was not possible to include the friction. In the Fig. 5 one can see the wedge positions and the resulting force on the motor spindle when the two springs were optimized with respect to each other. The secondary spring mimicking the leaf spring has a 0,1N preload and 0,22N/mm spring constant. For the primary extension spring the same values were 1,34N and 0,47N/mm, respectively. The results showed that the reaction force in z-direction can be well below 2N limit set by the motor and is fairly even over the full travel length of 9mm. Also the reaction force on the Fiber End Cap in z-direction was recorded and the resulting curve was the basis to design the leaf spring later in ANSYS.

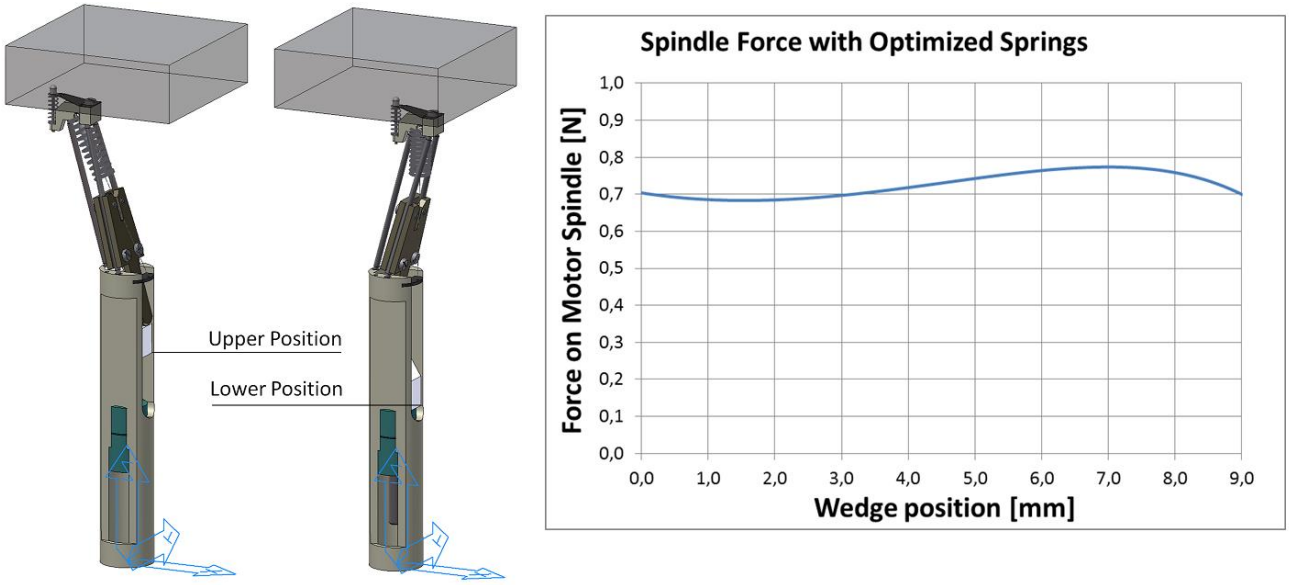

Figure 5. The resulting force on the linear motor spindle in Z-direction when the wedge is driven from its upper position down to its lower position by 9mm. The parameters of the two virtual springs are optimized to keep the force well below 2N and to have fairly even force distribution over the full length of travel. The force corresponds to static equilibrium at each wedge position and hence the frictional forces are not included.

Also the required torque for the rotational motor to keep the mechanism in static equilibrium with varying gravity vector conditions was simulated. However, because the holding torque of the θ-motor together with the gearbox assembly was enormous 1,63Nm it was not necessary to pursue with detailed analysis. The torque provided by the motor exceeded 7700 times the torque needed to keep the mechanism in static equilibrium.

5. FINITE ELEMENT ANALYSIS

Finite element analysis was carried out with ANSYS to calculate frictional effects, deformations and stresses in the dynamic mechanism. The task was not trivial due to large number of contacts, high friction coefficients, large displacements and large deformations that all introduced in nonlinear effects. As a result a great deal of effort was needed to get the model to converge. Therefore it is important here to address which contact parameters were used to achieve a working dynamic and nonlinear finite element model. The final contact parameters described here are result of literature studies, discussions with ANSYS specialists and trial and error.

For all sliding contacts the *Frictional*-type of contact had to be used in order to simulate frictional effects. Formulation of the *Pure Penalty* was chosen for the sliding contact between the ferrule and upper body. This type of contact prevents any penetration by modifying the present stiffness matrix by adding large terms in it. However, even this approach can be sensitive to contact stiffness and may lead to badly conditioned matrices, it was found to work the best for this particular contact[5].

The other contacts (foot-wedge, wedge-lever and fiber end cap-field-lens) took advantage of *Augmented Lagrange* multipliers. In this method the size of the stiffness matrix is increased by adding more DOF terms in it. Hence the contact pressure was taken to account which improved convergence and the calculation was less sensitive to contact stiffness[5]. However, because the stiffness matrix was now bigger it needed more iterations to reach equilibrium state.

For all of the defined contacts the *symmetric* behavior of contact was selected so that there was no matter which of the two combined surfaces were defined as a target or contact surface. This leads to faster computing times and improved convergence. The *Normal Stiffness Factor* was set manually to 0,1 because too large stiffness factors can lead to oscillating convergence[6].

The *Pinball Region* is a spherical region around each target or contact element. ANSYS checked whether the target and the contact elements were in-contact, near-contact or not near contact. This was helpful in the dynamic model because if the target and contact elements happened to separate, ANSYS could still find the elements and continue computing. The *Interface Treatment* was also set to *Adjust to Touch*, meaning that if there were some small separations or penetrations of surfaces in the imported 3D model, ANSYS automatically adjusted the surfaces into contact.

For the ferrule-upper body-contact additional *Stabilization Damping Factor* was set to stabilize the contact. This introduces a small viscous traction proportional to velocities between the surfaces[6]. In the Table 2 the contact parameters are summarized and in Table 3 some important material parameters that were used in the FEA are shown.

Table 2. Used contact parameters for the analysis

Contact	Foot-Wedge	Wedge-Lever	Ferrule-Upper Body	Ferrule-Field-lens
Friction Coefficient	0,2	0,2	0,15	0,1
Formulation	Augmented Lagrange	Augmented Lagrange	Pure Penalty	Augmented Lagrange
Interface Treatment	Adjust to Touch	Adjust to Touch	Adjust to Touch	Adjust to Touch
Normal Stiffness Factor	0,1	0,1	0,1	0,1
Stabilization Damping Factor	0	0	0,002	0
Pinball Radius	1mm	1mm	1,2mm	1mm

Table 3. Material properties used for analysis.

Material	Bodies	Density Kg/m^3	Young‘s Modulus [GPa]	Poisson’s Ratio	Tensile Yield Strength [MPa]
Spring Steel*	Leaf spring	7850	183	0,30	1852**

Stainless Steel	Foot Lever Back plate Upper body Shim Ferrule Field-lens	7750	193	0,31	207
Brass	Wedge Rods	8300	110	0,34	280

* Sandvik 11R51, cold rolled stainless steel[7] **$R_{p0,2}$

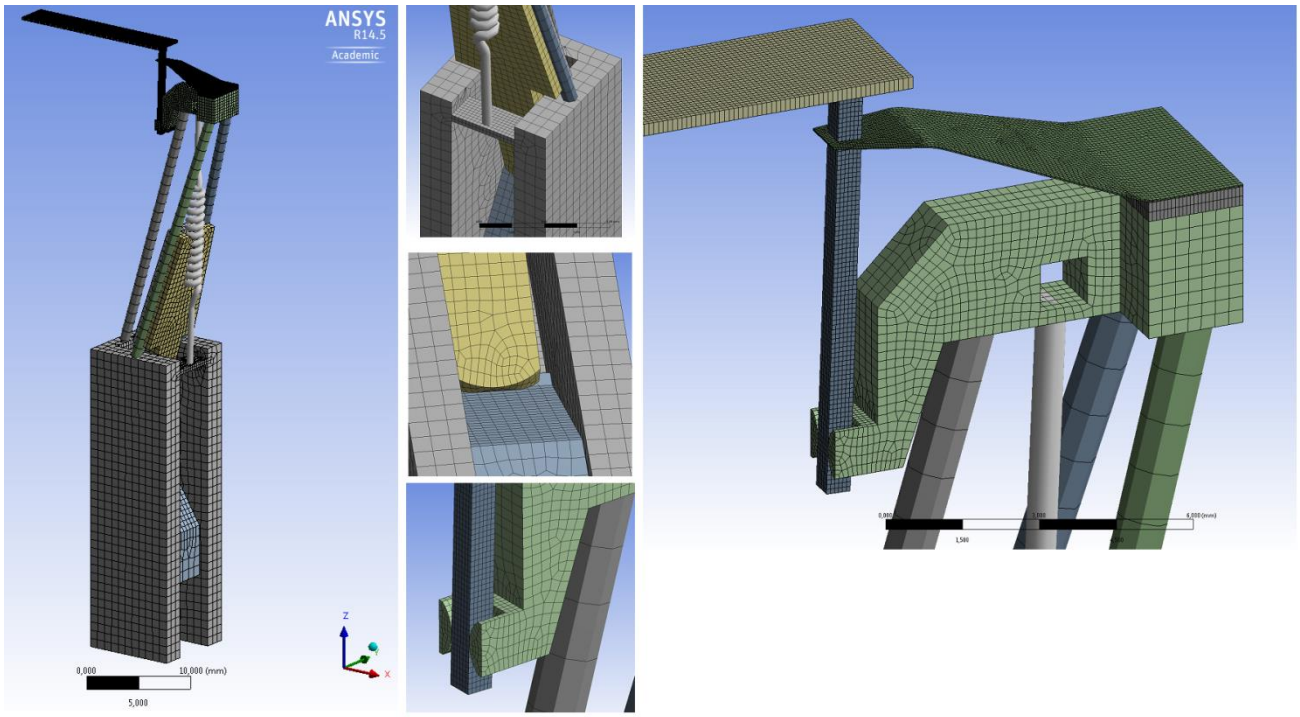

Figure 6. Mesh of the simplified 3D-model used for the analysis. The entire model has 151 155 nodes and 36 206 elements.

The calculation was done in three steps. In the first step the field-lens was lowered by 0,5mm (direction –z) in order to apply suitable preload for the leaf spring. The velocity of the field-lens was set to 0,25mm/s and after reaching its final position it was then kept fixed. In the next two steps the wedge was moved from its lower position 9mm upwards (direction +z) until it reached its uppermost position. It was important not to set too high displacement velocities. ANSYS is using the iterative Newton-Rapshon Method for the analysis and if the displacement is stepped too rapidly the force-displacement-curve of the method cannot be followed and a solution will not be found.

In the second step a velocity of 1mm/s was set for the wedge movement and it reached 7mm after 9s from the start of the simulation. Because the last 2mm was found to be difficult for ANSYS to converge the force, additional third step was added with a lower displacement velocity (0,5mm/s). In addition the number of substeps was increased from 100 to 150. The *Large Deflection* setting was turned on manually for each step. In total more than 2300 iterations were required to solve the entire model and it took 45h for the computer. The baseline for the force criterion is around 0,02N and it sets the fundamental accuracy for the calculated forces.

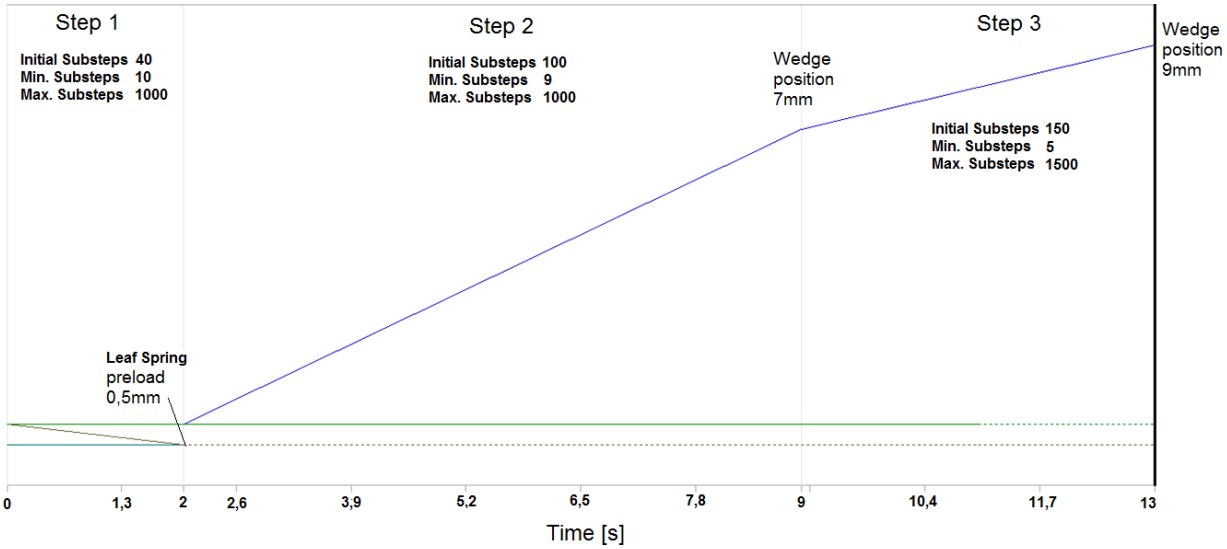

Figure 7. Displacement curves and steps used for the calculations.

It was clear that stress in the leaf spring was the most critical due to its large deformation. Therefore the first task was to optimize the spring so that it didn't exceed its yield strength and the reaction force on the Fiber End Cap was close to the optimized results showed by the static simulations. The optimum leaf spring thickness was only 0,04mm with the estimated maximum equivalent stress (von-Mises) 1200MPa as shown in the Fig 8. The results showed high localized stress at the corners of the ferrule cut but this was neglected because in the real model the opening is circular.

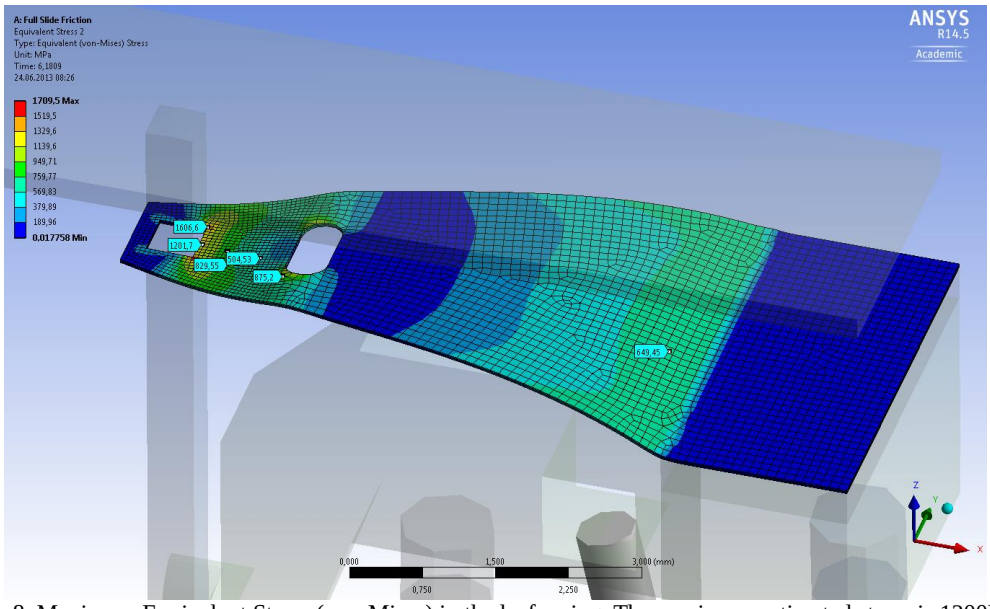

Figure 8. Maximum Equivalent Stress (von-Mises) in the leaf spring. The maximum estimated stress is 1200MPa because the localized high stress areas will be not present in the final spring which has a circular opening.

In the Fig. 9 (left) the reaction force on the motor spindle is shown as a function of wedge position. The average force is relatively constant over the entire travel length. This indicates that the two springs are well balanced with respect to each other. However, the force is unstable due to stick-and slip effects. The average value of the force is 1,81N having a standard deviation of 0,07N. The force calculated using FEA is significantly higher than the forces seen in the static

simulations. This indicates that friction and dynamic behavior noticeably increase the reaction force on the motor spindle. There seems to be also a transition area in the middle where the leg group is close to its straight vertical orientation. This could potentially cause some further positioning errors. The frictional contacts were clearly a difficult task for ANSYS to calculate and therefore also the results must be taken with caution. However, both static simulation and FEA showed reaction forces below 2N which is the specified stall force of the linear piezo motor.

Next the effects of the rotational θ-motion were under study. The analysis was slightly changed so that during the step 2 and 3 the field-lens was also moved with a velocity of 0,127mm/s in the direction +y. This applies a tangential friction force on the Fiber End Cap very much like a rotational movement. The resulting displacement of the contact point (ferrule-field-lens) from its nominal position in y-direction is shown in the Fig 9 (right). The maximum mean displacement can be found at the wedge position 2,8mm and is equivalent to 9,4µm. Due to stick- and slip effects the maximum amplitude of deformation is 7,12µm and it can be found close to the wedge position 2mm. The results of stick- and slip effect must be taken with caution since it depends on many parameters that are not well known. Only a prototype would give exact results. Due to hysteresis the entire maximum mean displacement is close to 18,8µm when the direction of rotation is changed. When the θ-motor positioning error was taken into account the total positioning error became ±11µm. Play due to ball bearings enabling the θ-motion has not been studied in detail. However, possibilities to use carefully pre-stressed high tolerance class bearings with minimum play has been discussed with bearing suppliers.

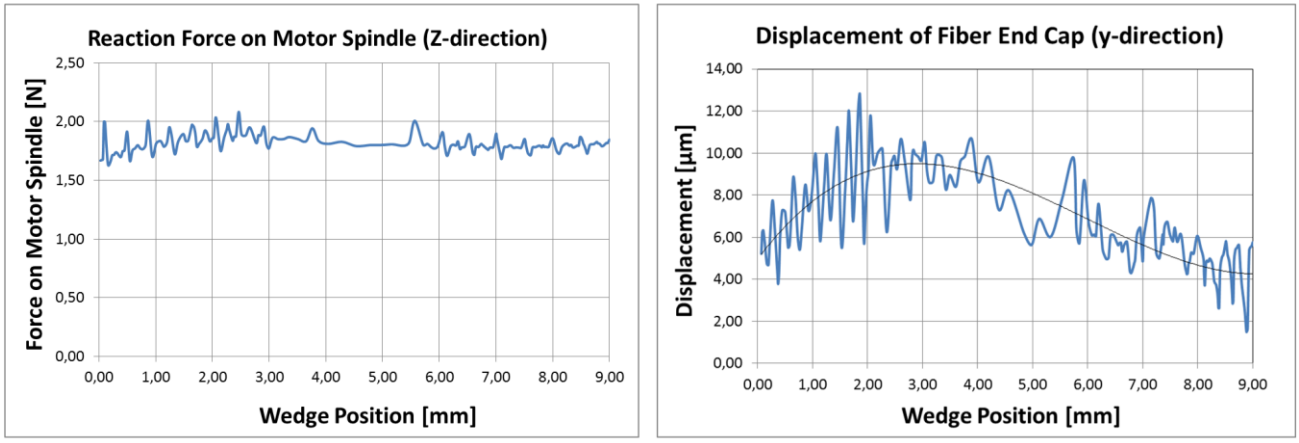

Figure 9. Left: reaction force on the motor spindle with dynamic movement and friction. The average value for the force is 1,81N and there is a transition area where the leg group is close to its straight vertical position. Right: displacement of the Fiber End Cap in y-direction simulating the θ-motion. Note that in both cases the wedge is now driven from its lower position to the upper position unlike in the static simulation.

To see the friction generated displacements in x-direction a different approach was required. A simplified analysis was set up. The field-lens was removed from the model. External friction force pointing to the direction -x was then applied on tip of the ferrule. The wedge was then moved from its lower position upwards to the direction +z in 5 steps. For each wedge position equivalent friction force was added. The friction forces were retrieved from the previous results. For the wedge position 3,97mm where the displacement had its maximum, more detailed analysis was pursued. The leaf spring was first lowered by 1,5mm and the equivalent friction force of 0,03N in +x-direction (positive direction showed larger displacements) was applied at the tip of the ferrule. The maximum displacement in x-direction is estimated to be 3,09µm. The estimation for the total positioning error of R-motion is ±4µm including frictional effects and the motor resolution. Deformations due to gravity were found to be in sub-micron level and can be therefore neglected.

The reaction forces were also studied in x-direction at the tip of the linear motor spindle. As it turned out due to the geometry and combination of force acting points a small torque emerged to the wedge about the axis y. The lower part of the wedge was lifted from the foot back surface while in lower wedge position because the friction force between the wedge and the spindle was not high enough to compensate the torque. A longer wedge could keep the wedge always in contact with the foot but this can't be easily done since it will then collide with the leg group. Another solution would be to use a tapered hole instead of the flat-bottom slot for the spindle. However, this would lead to more over-constrained mechanism and additional radial forces would be applied on the spindle. Maximum radial force is not specified by the

motor manufacturer and should be therefore tested. The third option would be to implement another leaf spring to push the wedge against the foot. The constraints are then maintained but the required motor force in z-direction must be then verified.

6. FURTHER DEVELOPMENT

It's clear that the PotsPos design is not mature enough to be adopted for an instrument build yet. In the next step it would be interesting to first solve the couple of design challenges that came out from the analysis. Namely the sliding wedge needs to be redesigned so that it doesn't lift off from the foot back surface and a new way to route the fiber should be found not to exceed the minimum bend radii. It would be then interesting to build the first prototype. Especially the frictional disturbances could be then studied in detail. Before PotsPos actuator is scalable to a full size fiber positioner the relatively complex design should be simplified by integrating some elements and functions. Also an alternative more cost-effective solution for the rotational θ-motor would be desired.

It might be also worthwhile to look back to the early PotsPos design with flexures. In recent years advanced 3D-printing technologies have emerged allowing composites of materials to be printed. There might be a solution where the main structural elements of PotsPos are made of hard plastic and embedded flexures are printed with softer material more suitable for large deformation. 3D-printing would be a very attractive choice because the manufacturing costs would decrease dramatically compared to the latest PotsPos design requiring machining of several parts.

7. SUMMARY

We have introduced a new R-θ actuator design for multi-object astronomical spectroscopy that is especially developed to meet the design requirements of the 4MOST. PotsPos was an alternative actuator design for the Echidna FMOS tilting spine actuator concept currently chosen for the 4MOST. The main advantages over the tilting spine design are that PotsPos does not suffer from focal ratio degradation and defocus issues introduced in by the fiber tilt. The length of the actuator is also shorter and it fits more easily to tight space envelope of the 4MOST positioner. PotsPos maintains good fiber assignment flexibility and large fill factor with a 10mm pitch in a regular hexagonal grid. Thanks to its large 28mm patrol diameter it has better overlap with surrounding patrol areas compared to θ-Phi actuator concepts.

The early PotsPos design based on bending flexures was introduced and was followed by a description of the new PotsPos design that takes advantage of play-free spherical joints rather than flexures. The feasibility of this design was studied in detail using several analyzing tools. The results showed that with optimized preloaded springs the reaction force on the piezo-electric linear motor can be kept below 2N limit. The selected rotational θ-motor integrated with one planetary gear and one harmonic drive provided high enough positioning accuracy. When motor resolutions and actuator deformations due to frictional forces were taken into account the calculated positioning accuracy for the R-motion became ±4µm and for the θ-motion ±11µm, respectively. Before the first prototype could be built to examine the real frictional disturbances some small design modifications would be needed to have a well working mechanism.

ACKNOWLEDGMENTS

We gratefully acknowledge the financial support of the German Federal Ministry of Education and Research (BMBF) through the Verbundforschung (grant no. 05A11BA3) and the Program Unternehmen Region (grant no. 03Z2AN11).

REFERENCES

[1] de Jong, R. S., Bellido-Tirado, O., Chiappini, C., Depagne, É., Haynes, R., Johl, D., Schnurr, O., Schwope, A., Walcher, J., Dionies, F., Haynes, D., Kelz, A., Kitaura, F. S., Lamer, G., Minchev, I., Müller, V., Nuza, S. E., Olaya J., Piffl, T., Popow, E., Steinmetz, M., Ural, U., Williams, M., Winkler, R., Wisotzki, L., Ansorge, W. R., Banerji, M., Solares, E. G., Irwin, M., Kennicutt, R. C., King, D., McMahon, R. G., Koposov, S., Parry, I. R., Sun, D., Walton, N. A., Finger, G., Iwert, O., Krumpe, M., Lizon, J., Vincenzo, M.; Amans, J., Bonifacio, P., Cohen, M., Francois, P., Jagourel, P., Mignot, S. B., Royer, F., Sartoretti, P., Bender, R., Grupp, F., Hess, H., Lang-Bardl, F.,

Muschielok, B., Böhringer, H., Boller, T., Bongiorno, A., Brusa, M., Dwelly, T., Merloni, A., Nandra, K., Salvato, M., Pragt, S. M., Navarro, R., Gerlofsma, G., Roelfsema, R., Dalton, G., B., Middleton, K. F., Tosh, I. A., Boeche, C., Caffau, E., Christlieb, N., Grebel, E. K., Hansen, C., Koch, A., Ludwig, H., Quirrenbach, A., Sbordone, L., Seifert, W., Thimm, G., Trifonov, T., Helmi, A., Trager, S. C., Feltzing, A., Korn, A., Boland, W., "4MOST – 4-metre Multi-Object Spectroscopic Telescope," Proc. SPIE 8446, (2012).

[2] Saviauk, A., "Mechanical design and simulation of PotsPos optical fiber actuator for multiobject astronomical spectroscopy," Master's Thesis, Ernst-Abbe Fachhochschule Jena / AIP (2013).

[3] New Scale Technologies Inc., "SQL-3.4 Linear Micro Motor for OEM Product Applications," <http://www.newscaletech.com/doc_downloads/SQL-3-4_Motor_datasheet.pdf> (07 May 2014).

[4] Dr. Fritz Faulhaber GmbH & Co. Kg., "Miniature Drive Systems," p. 248, Edition 2014 <http://www.faulhaber.com/Catalogue/DE/page248.html#/248> (07 May 2014).

[5] Johnson, D. H., "Principles of simulating contact between parts using ANSYS," <http://ansys.net/ansys/papers/nonlinear/principles_of_simulating_contact_between.pdf > (7 May 2014).

[6] Higgins, J., "Obtaining and Optimizing Structural Analysis Convergence," ANSYS Inc., 2012, <http://www.ansys.com/staticassets/ANSYS/Conference/Confidence/Boston/Downloads/obtaining-and-optimizing-convergence.pdf> (7 May 2014).

[7] Sandvik Materials Technology, "Sandvik Santronic Handbook," p. 14, <http://www.smt.sandvik.com/Global/Downloads/Products_downloads/strip-steel-and-strip-based-products/sandvik-santronic-pre-coated-strip/sandvik-santronic-handbook/sandvik-santronic-pre-coated-strip(S-SY016-B_081029_2).pdf> (7 May 2014).